

Diffuse and Gravitationally Stable Molecular Gas in the Post-Starburst Galaxy NGC 5195

Kotaro KOHNO

Institute of Astronomy, The University of Tokyo, 2-21-1, Osawa, Mitaka, Tokyo 181-8588
kkohno@ioa.s.u-tokyo.ac.jp

Tomoka TOSAKI

Gunma Astronomical Observatory, Nakayama, Takayama, Agatsuma, Gunma 377-0702
tomoka@astron.pref.gunma.jp

Satoki MATSUSHITA

Submillimeter Array, Harvard-Smithsonian Center for Astrophysics,
P.O. Box 824, Hilo, HI 96721-0824, U.S.A.
smatsu@sma.hawaii.edu

Baltasar VILA-VILARÓ

Steward Observatory, The University of Arizona, Tucson, AZ 85721, U.S.A.
bvila@as.arizona.edu

Toshihito SHIBATSUKA

Nobeyama Radio Observatory, Minamimaki, Minamisaku, Nagano 384-1305
Department of Astronomy, The University of Tokyo, 7-3-1 Hongo, Bunkyo-ku, Tokyo 113-0033
shiba@nro.nao.ac.jp

and

Ryohei KAWABE

National Astronomical Observatory, 2-21-1, Osawa, Mitaka, Tokyo 181-8588
kawabe@nro.nao.ac.jp

(Received 2000 September 7; accepted 2002 May 12)

Abstract

The Nobeyama Millimeter Array (NMA) has been used to make aperture synthesis CO(1–0) observations of the post-starburst galaxy NGC 5195. CO(1–0) and HCN(1–0) observations of NGC 5195 using the Nobeyama 45 m telescope are also presented. High-resolution ($1''.9 \times 1''.8$ or $86 \text{ pc} \times 81 \text{ pc}$ resolution at $D = 9.3 \text{ Mpc}$) NMA maps show a strong concentration of CO emission toward the central a few \times 100 pc region of NGC 5195, despite the fact that the current massive star formation is suppressed there. The face-on gas surface density, Σ_{gas} , within the $r < 2''$ or 90 pc region reaches $3.7 \times 10^3 M_{\odot} \text{ pc}^{-2}$ if a Galactic $N_{\text{H}_2}/I_{\text{CO}}$ conversion factor is applied. The extent of the central CO peak is about $5''$, or 230 pc, and is elongated along the

E–W direction with two-armed spiral-like structures, which are typical for barred disk galaxies. The HCN-to-CO integrated intensity ratio on the brightness temperature scale, $R_{\text{HCN/CO}}$, is about 0.02 within the central $r < 400$ pc region. This $R_{\text{HCN/CO}}$ is smaller than those in starburst regions by a factor of 5 – 15. These molecular-gas properties would explain why NGC 5195 is in a post-starburst phase; most of the *dense* molecular cores (i.e., the very sites of massive star formation) have been consumed away by a past starburst event, and therefore a burst of massive star formation can no longer last, although a large amount of *low density* gas still exists. We find a steep rise of the rotation velocity toward the center of NGC 5195. As a consequence, the critical gas surface density for a local gravitational instability of the gas disk becomes very high ($\Sigma_{\text{crit}} \sim 6.9 \times 10^3 M_{\odot} \text{ pc}^{-2}$), suggesting that the molecular gas in the central region of NGC 5195 is gravitationally *stable*, in contrast to that of starburst galaxies. We propose that dense molecular gas can not be formed from remaining diffuse molecular gas because the molecular gas in the center of NGC 5195 is *too stable* to form dense cores via gravitational instabilities of diffuse molecular gas. The deduced very high threshold density seems to be due to a high mass concentration in NGC 5195. The known trends on the occurrence and luminosity of nuclear star formation in early-type galaxies can be understood naturally if the high threshold density is characteristic for early-type galaxies.

Key words: galaxies: individual(NGC 5195) — galaxies: ISM — galaxies: elliptical and lenticular, cD — galaxies: starburst

1. Introduction

Recent studies on the molecular-gas properties in galaxies have revealed an intimate relationship between starbursts and high-density ($n_{\text{H}_2} > 10^4 \text{ cm}^{-3}$) molecular gas; quantitative correlations between HCN(1–0) emission, which is an indicator of dense molecular gas contents, and star-formation tracers, such as a far-infrared (FIR) continuum and radio recombination lines, have been demonstrated (e.g., Solomon et al. 1992; Zhao et al. 1996; Paglione et al. 1997). High-resolution images of HCN(1–0) emission with millimeter-wave arrays also show spatial coincidence of dense molecular material with the massive star-forming regions in starburst/star-forming galaxies (e.g., Paglione et al. 1995; Kohno et al. 1999, but see Aalto et al. 2001).

Given the important role of dense molecular matter on massive star-formation, it would be then important to investigate how they are formed. A nonaxisymmetric distortion of the underlying potential in galaxies caused by various dynamical effects, such as disk instability and galaxy–galaxy interactions (e.g., Noguchi 1996), is often invoked as an efficient mechanism which stirs interstellar matter (ISM) on the large scale (from a few to a few $\times 10$ kpc) disk of

galaxies into the very central (a few \times 100 pc) regions by removing the angular momentum of ISM (e.g., Shlosman et al. 1989). To date, however, the physical process which could transform *diffuse* ISM into dense molecular gas has not been addressed so often. Moreover, most of the observational studies on dense molecular gas have concentrated on luminous starburst galaxies, such as NGC 253 and M 82. It must be valuable to assess the distribution and physical properties of molecular gas in *quiescent* and *less star-forming* galaxies in order to seek a clue on dense gas formation.

In this paper, we report on high-resolution aperture synthesis CO(1–0) observations and simultaneous CO(1–0) as well as HCN(1–0) spectroscopy of the early-type barred galaxy NGC 5195, made with the Nobeyama Millimeter Array (NMA) and NRO 45 m telescope. As described below, NGC 5195 may be one of the ideal targets to investigate the molecular-gas properties in the galaxy whose star formation is currently at a very low level; NGC 5195 is a barred lenticular galaxy (SB0 pec; Sandage, Tammann 1981) at a distance of 9.3 Mpc (Tully 1988), known as a companion of the well-studied spiral galaxy M 51/NGC 5194. In spite of the abundant molecular gas in the central region of NGC 5195 (Sage, Wrobel 1989; Sage 1989, 1990; Aalto, Rydbeck 2001), the current massive star-formation seems to be suppressed there. Narrow-band imaging does not show any significant H α *emission*, and strong H α *absorption* dominates in the central $\sim 10''$ region instead (Thronson et al. 1991; Sauvage et al. 1996; Greenawalt et al. 1998; see also optical spectra by Filippenko, Sargent 1985). This Balmer absorption feature is attributed by a presence of numerous A-type stars, and few stars earlier than A4 exist in this region (Rieke 1988; Yamada, Tomita 1996). Considering the lifetime of A-type stars (from a few $\times 10^8$ to 10^9 yr) and the typical duration of starbursts (a few $\times 10^7$; Thornley et al. 2000 and references therein), it is strongly suggested that NGC 5195 experienced a nuclear starburst about ~ 1 Gyr before, and is now in the *post-starburst phase*, where the OB stars produced by the starburst event have disappeared and only late-type stars (A stars and later) remain in this region. This situation is strikingly similar to the archetypical post-starburst galaxy NGC 4736 (Pritchett 1977; Rieke et al. 1988; Walker et al. 1988; Taniguchi et al. 1996). A mid-infrared (MIR) study with ISOCAM by Boulade et al. (1996) has also revealed the post-starburst nature of NGC 5195. Consequently, the current star-formation rate (SFR) is very small; the H α emission luminosity can be found by subtracting the underlying absorption feature by A stars, and is estimated to be 8.7×10^{37} erg s $^{-1}$ within a $2'' \times 4''$ aperture (Ho et al. 1997a). This is near the lowest end of $L(\text{H}\alpha)$ in their sample, containing about 500 nearby galaxies in the northern hemisphere. Note that optical spectroscopy suggests the nucleus of NGC 5195 may be a LINER (e.g., Ho et al. 1997a), which could be a signature of a low-luminosity active galactic nucleus (AGN). Radio and MIR observations also show a compact and luminous source in the center of NGC 5195 (van der Hulst et al. 1988; Boulade et al. 1996). It is, however, unclear whether a compact non-stellar powered source exists in the nucleus of NGC 5195, because neither a compact UV core (Barth et al. 1998) nor ionized neon lines in the

MIR band (Boulade et al. 1996), both are characteristic features of an AGN, has been detected. High-angular resolution X-ray observations of NGC 5195 also reveal an extended distribution of hot gas (Ehle et al. 1995; Georgantopoulos et al. 2002), in favour of a star-forming origin for the bulk of the X-ray emission. The radio and MIR concentrations, therefore, would be related to past starburst events (SNRs and hot dust heated by late-type stars). The parameters of NGC 5195 are listed in table 1.

2. Observations and Data Reductions

2.1. NRO 45 m Observations

We performed simultaneous HCN(1–0) and CO(1–0) observations toward the center of NGC 5195 using the NRO 45 m telescope on 1996 December. In order to avoid the degradation of any beam pattern, beam efficiency, or pointing accuracy of the telescope, the observed data were discarded if the wind velocity exceeded about 4 m s^{-1} . The full widths of the half-power beam (FWHP) were $15''$ and $19''$ at the observed frequencies of CO and HCN, respectively. The main-beam efficiency, η_{MB} , was about 0.5 at the 3 mm band. We used two cooled SIS mixer receivers, S80 and S100, equipped with side-band rejection filters, and observed both the CO and HCN lines simultaneously. The beam squint of the two receivers had been aligned to less than $2''$. Absolute pointing of the antenna was checked every hour using SiO maser sources, and the pointing accuracy was better than $\pm 4''$ (peak-to-peak). The typical system noise temperature for CO and HCN observations were about 800 K and 300 K in the single side-band, respectively. The sky emission was subtracted by position switching with an off-source position at an offset in the azimuth of $8'$ from the observed position. The spectra of CO and HCN emission were obtained with 2048 channels acousto-optical spectrometers of 250 MHz bandwidth, corresponding to a velocity coverage of 650 km s^{-1} for CO observations, and 850 km s^{-1} for HCN observations. After removing linear baselines from the spectra, adjacent channels were averaged. The resultant velocity resolution is 10 km s^{-1} for CO and 30 km s^{-1} for HCN. The 45 m telescope observations are summarized in table 2.

2.2. NMA Observations

NMA observations of CO(1–0) emission in the central region of NGC 5195 were made during the period from 1999 November to 2000 March. The NMA consists of six 10 m antennas equipped with cryogenically cooled SIS mixer receivers. Three available array configurations (AB, C, and D) were used. Due to the limitation of the minimum projected baseline length (10 m), extended structures larger than about $50''$ in each channel map were not sampled in the observations. The receiver noise temperatures at the 3 mm band were 20 – 40 K in the double side-band, and the system noise temperatures in the single side-band were about 800 K toward the zenith. The Ultra Wide-Band Correlator (UWBC; Okumura et al. 2000) was configured to cover 512 MHz with 256 channels per baseline. Side-band separation was achieved by 90°

phase switching. We observed the quasar 1418+546 every ~ 30 min in order to calibrate the temporal variations of the visibility amplitude and phase. The passband across 256 channels was calibrated through observations of a strong continuum source, 3C 279. The flux density of the reference calibrator was determined from comparisons with planets of known brightness temperatures. It ranged from 0.5 to 0.7 Jy during the observation period, and the uncertainty in the absolute flux scale was about $\pm 20\%$. The raw data were calibrated and edited using the package UVPROC-II developed at NRO (Tsutsumi et al. 1997), and Fourier-transformed using the AIPS task IMAGR. We produced two CO data cubes with different imaging parameters; one was maps using a natural weighting by applying a $80\text{ k}\lambda$ taper to the visibilities, and longer baseline visibilities ($> 80\text{ k}\lambda$) were cut. This resulted in a moderate spatial resolution of $4''.7 \times 3''.2$ (P.A. = -54°). The other cube was made using a robust weighting (robust parameter = 0) to achieve a high angular resolution ($1''.9 \times 1''.8$). Hereafter, we refer to these two cubes as “low resolution” and “high resolution”, respectively. A conventional CLEAN method was applied to deconvolve the synthesized beam pattern. Summaries of the observations and the parameters of the CO data are listed in table 3.

3. Results

3.1. NRO 45 m Observations

We detected strong CO(1–0) emission in the center of NGC 5195, whereas HCN(1–0) emission was found to be very weak. The CO and HCN spectra are shown in figure 1, and the quantities derived from these spectra are summarized in table 2.

The CO profile shows two velocity features, i.e., a $400 - 450\text{ km s}^{-1}$ component and a $450 - 750\text{ km s}^{-1}$ component, which are mostly consistent with the earlier CO detection (Sage 1990). It has been suggested that the lower velocity component is from the spiral arm of M 51, a companion of NGC 5195, and that the higher velocity component is associated with NGC 5195 itself. A high-resolution NMA map of CO(1–0) emission, presented in the following section, confirms this picture. The velocity-integrated CO intensity, $I(\text{CO}) = 83\text{ K km s}^{-1}$, corresponds to a face-on molecular gas surface density of about $430 M_\odot\text{ pc}^{-2}$, adopting the formula

$$\Sigma_{\text{H}_2} = 4.81 \times \cos i \cdot \left(\frac{I_{\text{CO}}}{\text{K km s}^{-1}} \right) \left[\frac{X_{\text{CO}}}{3.0 \times 10^{20}\text{ cm}^{-2} (\text{K km s}^{-1})^{-1}} \right] \quad (1)$$

and

$$\Sigma_{\text{gas}} = 1.36 \times \Sigma_{\text{H}_2}, \quad (2)$$

where i is the inclination of the disk ($i = 37^\circ$ here), I_{CO} is the velocity-integrated CO intensity, and X_{CO} is the $N_{\text{H}_2}/I_{\text{CO}}$ conversion factor (Scoville et al. 1987; Solomon et al. 1987).

We find that the HCN emission in the center of NGC 5195 is very weak. Because the detection was about the 3σ level, it should be regarded as tentative. The HCN-to-CO integrated intensity ratio in brightness temperature scale, $R_{\text{HCN/CO}}$, is given as about 0.02.

Note that the beam sizes of CO and HCN observations are slightly different (15'' and 19'', respectively), and one should note that such a difference could cause an error in the estimation of the intrinsic gas properties.

3.2. NMA Observations

3.2.1. Molecular-gas distribution and kinematics in NGC 5195

Figure 2 shows velocity channel maps of the low-resolution CO data cube in the central $50'' \times 50''$ (corresponding to 2.3 kpc at $D = 9.3$ Mpc) area of NGC 5195. CO emission is clearly detected ($> 4\sigma$) over the velocity range from 487 to 737 km s^{-1} , and presumably detected even in the 471 and 752 km s^{-1} channels.

A velocity-integrated CO map (the high resolution data) over the 471 – 752 km s^{-1} range is shown in figure 3c, along with an intensity-weighted mean-velocity map in figure 3d. CO maps made from the low-resolution data cube are shown in figure 4. These 0th and 1st moment maps were produced using the AIPS task MOMNT, with a clip level of 1.5σ in each channel. We can immediately see a strong concentration of CO emission toward the nucleus of NGC 5195. The azimuthally averaged radial distribution of molecular gas shown in figure 5, which was calculated using the AIPS task IRING, suggests that the peak gas mass per unit area including He and heavier elements, Σ_{gas} , reaches about $3.7 \times 10^3 M_{\odot} \text{pc}^{-2}$, adopting the equations (1) and (2). The Σ_{gas} derived here is much higher than that from the 45 m data. This is solely due to the dilution effect; the beam filling factor of molecular emission is very small.

The CO peak corresponds to the radio peak position, and is mostly associated with the $\text{H}\alpha$ absorption region, which can be seen in figure 3b. In this region, a hot dusty ring has also been discovered by a B-15 μm color map (Block et al. 1997), and which could also be a reminiscent of a past starburst event. The relationship between molecular gas and the past starburst in the center of NGC 5195 is discussed in section 4.

The CO flux, S_{CO} , within the central $r < 500$ pc (11'') region in figure 4 is 280 Jy km s^{-1} , and the total flux detected in the F.O.V. is about 380 Jy km s^{-1} . These correspond to a molecular gas mass of $4.0 \times 10^8 M_{\odot}$ and $5.4 \times 10^8 M_{\odot}$, respectively, following the equations

$$M(\text{H}_2) = 1.2 \times 10^4 \left(\frac{S_{\text{CO}}}{\text{Jy km s}^{-1}} \right) \left(\frac{D}{\text{Mpc}} \right)^2 \left[\frac{X_{\text{CO}}}{3.0 \times 10^{20} \text{ cm}^{-2} (\text{K km s}^{-1})^{-1}} \right] \quad (3)$$

and

$$M(\text{gas}) = 1.36 \times M(\text{H}_2). \quad (4)$$

The averaged gas surface density within the $r < 500$ pc region is $\Sigma_{\text{gas}}(r < 500 \text{ pc}) = 5.0 \times 10^2 M_{\odot} \text{pc}^{-2}$. This Σ_{gas} is comparable to those in a normal spiral survey (Sakamoto et al. 1999b), which consists of 20 CO-luminous spiral galaxies with morphology types from Sa to Sd. Note that the number of S0 galaxies where high-resolution CO images are available is still limited to date (e.g., NGC 4701, Wrobel, Kenney 1992; NGC 404, Cepa et al. 1998; NGC 3593, Sakamoto et

al. 1999a; NGC 7465, Kohno et al. 2001), though a large number of CO detections have been reported (e.g., Sage, Wrobel 1989; Thronson et al. 1989; Tacconi et al. 1991; Taniguchi et al. 1994). Our results suggest that some S0 galaxies can contain a large amount of molecular gas comparable to disk galaxies.

The CO velocity field in the low-resolution map (figure 4) seems to be dominated by circular rotation. A simple fitting of the observed velocity field with the AIPS task GAL gives a systemic velocity of about $628 \pm 5 \text{ km s}^{-1}$ and a P.A. of the kinematic major axis of about $+106^\circ \pm 3^\circ$ (measured counterclockwise from north), although it can depend on the area where the fitting is made. The P.A. is mostly consistent with the value in RC3 (table 1). On the other hand, the systemic velocity derived here differs significantly from the HI velocity listed in RC3, $465 \pm 10 \text{ km s}^{-1}$. Our CO measurements must be more accurate, because high-resolution observations of HI do not show any significant HI emission in the center of NGC 5195 (Rots et al. 1990), and the listed HI velocity in RC3 seems to be contaminated by the HI from M 51.

A position-to-velocity map (pv map) along the kinematic major axis (P.A. = $+106^\circ$) is displayed in figure 6. We find a steep rise of rotation velocity on the pv map; it reaches about 160 km s^{-1} at $r \sim 1''$ or 45 pc on the plane of the galaxy, adopting $i = 37^\circ$. Note that we see a velocity component near $V_{\text{LSR}} \sim 430 \text{ km s}^{-1}$, which may be CO emission associated with M 51 (see 3.2.2).

The observed gas morphology is reminiscent of those in barred spiral galaxies (e.g., Kenney et al. 1992; Sakamoto et al. 1995; Reynaud, Downes 1997; Regan et al. 1999); two offset ridges emanate from the central gas concentration, and are connected to curved structures. A curved or spiral-like feature, which can often be a signature of the gas orbit resonance in barred galaxies, is particularly evident in the NW part. In fact, near-infrared (NIR) photometry clearly shows the presence of a large-scale stellar bar along the N–S direction (Smith et al. 1990; Thronson et al. 1991; Spillar et al. 1992; Block et al. 1994); it is very natural to have an idea that they govern the gas distribution. If we assume that these are bar-induced structures, indeed, it is possible to specify the direction of rotation on the plane of the galaxy. In figure 7, we suggest a possible configuration. As can be seen in the figure, the northern part of the galaxy is suggested to be the near side, which is consistent with results obtained by assuming the outer spiral arms seen in NIR are trailing (Block et al. 1994). In order to fully understand the gas distribution and kinematics in the center of NGC 5195, detailed analyses on gas kinematics, including a comparison with the hot dusty ring (Block et al. 1997), will be needed.

3.2.2. *Low-velocity component, possible CO emission from M 51*

It should be noted that low-level ($3 - 4 \sigma$) emission can be seen near to the edge of the NMA F.O.V. (mostly the S–E portion of the F.O.V.) in the channel maps of the low-resolution CO cube (figure 2) for the velocity range $V_{\text{LSR}} = 378 - 440 \text{ km s}^{-1}$. If we correct the primary beam attenuation near the edge of F.O.V., these low-velocity emissions could be about 200

mJy beam⁻¹ or 1 K at the observing beam ($4''.7 \times 3''.2$). The velocity range of these low-level CO emissions is mostly the same as that of the low-velocity component detected at 45 m (and NRAO 12 m by Sage 1990). We show the integrated intensity map for the 378 to 440 km s⁻¹ range in figure 8. A peak near the S–E edge of the F.O.V. can be clearly seen in the figure, and this could be CO emission from M 51. This low-level emission is clearly depicted by recent multi-pointing imaging of the NGC 5195 region using the OVRO millimeter array (Aalto, Rydbeck 2001). Nevertheless, the flux ratio between 45 m and NMA data is very small for this velocity range, as can be seen in figure 9, which compares the 45 m and NMA spectra, although most of the CO emission from NGC 5195 itself seems to be recovered with the NMA observations. We therefore suggest that the CO emission from M 51 seen as the low-velocity component would be spread over a wide area of arcminutes scale, and that most of the low-velocity CO emission is resolved out in our interferometric observations. This seems to be consistent with the pv map by Sage (1990), which shows extended emission over a few arcminutes for the velocity component near $V_{\text{LSR}} \sim 400 \text{ km s}^{-1}$.

4. Discussions

The NMA observations of CO emission reveal that the post-starburst galaxy NGC 5195 does contain a significant amount of molecular gas, despite the fact that the current massive star formation is very inactive there; the molecular gas mass per unit area reaches about $\Sigma_{\text{gas}} \sim 3.7 \times 10^3 M_{\odot} \text{ pc}^{-2}$, which is comparable to those in nearby starburst galaxies. On the other hand, the star formation rate (SFR) per unit area, Σ_{SFR} , which was calculated from $2'' \times 4''$ aperture H α data (Ho et al. 1997a), is only about $\Sigma_{\text{SFR}} \sim 3.7 \times 10^{-8} M_{\odot} \text{ yr}^{-1} \text{ pc}^{-2}$ (table 1). This SFR is smaller than those in typical starburst galaxies by an order of magnitude (e.g., Kennicutt 1998a). The resultant gas consumption time scale,

$$\tau_{\text{gas}} = \frac{\Sigma_{\text{gas}}}{\Sigma_{\text{SFR}}}, \quad (5)$$

is about $\sim 9 \times 10^{10} \text{ yr}$, which is indeed comparable to τ_{gas} in quiescent or normal galaxies, and significantly longer than those in infrared-luminous starburst galaxies (e.g., Kennicutt 1998a). In the following section we discuss the possible relationship between the physical properties of molecular gas and star formation in the center of NGC 5195.

4.1. Decrease of Dense Molecular Gas in the Nucleus of the Post-Starburst Galaxy NGC 5195

We observed a very low $R_{\text{HCN/CO}}$ value of 0.02 in the center of NGC 5195. This is smaller than those in starburst galaxies by a factor of 5 – 15. For instance, $R_{\text{HCN/CO}}$ in NGC 253 is reported to be in the range of 0.2 – 0.3 (Helfer, Blitz 1993; Paglione et al. 1995; Sorai et al. 2000), and starburst galaxies such as NGC 6946 and IC 342, which are less active compared with NGC 253 in terms of FIR luminosities, show $R_{\text{HCN/CO}}$ values of about 0.1 (Downes et al. 1992; Helfer, Blitz 1997). $R_{\text{HCN/CO}}$ values in the circumnuclear starburst regions of NGC 1068

(Helfer, Blitz 1995) and NGC 6951 (Kohno et al. 1999) are also about 0.1 or so.

Because the critical gas density for collisionally excitation of HCN(1–0) emission ($n_{\text{H}_2} > 10^4 \text{ cm}^{-3}$) is much higher than that of CO(1–0) ($n_{\text{H}_2} \sim \text{a few} \times 10^2 \text{ cm}^{-3}$), a comparison of the CO and HCN intensities is a measure of the gas density if both of the CO and HCN emission originate from the same volume. In observations of galaxies, the observing beams are often too large to resolve the individual cloud structures, and $R_{\text{HCN/CO}}$ could indicate the fraction of dense molecular gas to the total (including diffuse) molecular gas within the observing beam (Kohno et al. 1999).

With this interpretation of $R_{\text{HCN/CO}}$ in galaxies, our data on NGC 5195 and its comparison with starburst galaxies would indicate that *the mass fraction of dense molecular components to the total molecular gas*, which is traced by the $R_{\text{HCN/CO}}$ values, *in the center of NGC 5195 is significantly small compared with that of starburst galaxies*. We suggest that this would be a reason why NGC 5195 is in a post-starburst phase despite the fact that it contains a large amount of molecular gas there; most of the dense molecular cores, which are the very sites of massive star formation, have been consumed away by starburst events which began about 1 Gyr before (see section 1). Also, a burst of massive star formation can no longer last, although a large amount of *diffuse* molecular gas remains there.

We should note that the $R_{\text{HCN/CO}}$ values often depend on the aperture size of the observations, and attention must be paid to derive the intrinsic properties of molecular gas from the $R_{\text{HCN/CO}}$ values. (e.g., Helfer, Blitz 1993; Jackson et al. 1996). For instance, $R_{\text{HCN/CO}}$ in the center of M 51 is 0.033 (Helfer, Blitz 1993) by the NRAO 12 m telescope (55'' for CO, and 71'' for HCN), whereas it becomes about 0.08 (Sorai et al. 2002) by the NRO 45 m telescope (15'' and 19'' for CO and HCN, respectively). In higher resolution (7'') observations, it reaches about 0.3 or more (Kohno et al. 1996). These effects are mostly due to the compactness of the HCN emitting regions, and therefore high-resolution observations are essential in order to address the relationship between dense molecular gas and massive star-forming regions. In the case of our NGC 5195 observations, the observing beams (15'' for CO and 19'' for HCN) correspond to aperture areas of $r < 340 \text{ pc}$ and $r < 430 \text{ pc}$ for CO and HCN, respectively. Small $R_{\text{HCN/CO}}$ values of less than 0.05 have been reported in various galaxies (e.g., Helfer, Blitz 1993; Aalto et al. 1995), but are mostly observed with a much larger beam size ($\sim 1'$) than ours, corresponding to a few \times kpc aperture area in their samples. We therefore suggest that the observed small $R_{\text{HCN/CO}}$ value in the central a few $\times 100 \text{ pc}$ of NGC 5195 is not the aperture size effect but reflects the intrinsic property of molecular gas, i.e., a decrease of dense molecular gas there. Our interpretation of a low $R_{\text{HCN/CO}}$ ratio seems to be supported by a low CO(2–1)/CO(1–0) ratio in NGC 5195; Sage (1990) observed CO(2–1) and CO(1–0) lines toward the center of NGC 5195 using the NRAO 12 m telescope, and found that the CO(2–1)/CO(1–0) ratio is as small as 0.5. They concluded that the molecular clouds in NGC 5195 are *less dense* than those in typical spiral galaxies.

4.2. Gravitationally Stable Molecular Gas Disk in the Center of NGC 5195

Given the close relationship between dense molecular gas and massive star formation/starburst, what kind of physical processes can play a major role in the formation of *dense* molecular clouds from a *low-density* molecular medium? One of the key processes could be gravitational instabilities of molecular gas; it is well known that SFR in the disk regions (\sim a few kpc scale) of galaxies can be described by means of the Schmidt law, $\Sigma_{\text{SFR}} \propto \Sigma_{\text{gas}}^{1.4 \pm 0.15}$, where Σ_{SFR} is the SFR per unit area, and Σ_{gas} is the gas mass per unit area (Kennicutt 1998a). Here it should be noted that the Schmidt law is valid only if the gas in the disk is gravitationally *unstable*, i.e., the gas surface density, Σ_{gas} , exceeds the critical gas surface density, Σ_{crit} , given by

$$\Sigma_{\text{crit}} = \alpha \frac{\sigma_v \kappa}{\pi G} = 73.9 \times \left(\frac{\alpha}{1}\right) \left(\frac{\sigma_v}{\text{km s}^{-1}}\right) \left(\frac{\kappa}{\text{km s}^{-1} \text{ pc}^{-1}}\right) M_{\odot} \text{ pc}^{-2}, \quad (6)$$

where α is a dimensionless constant close to unity¹, σ_v is the velocity dispersion in the radial direction, and κ is the epicyclic frequency,

$$\kappa = \left\{ 2 \frac{v(r)}{r} \left[\frac{v(r)}{r} + \frac{dv(r)}{dr} \right] \right\}^{0.5}, \quad (7)$$

where r is the distance from the center and $v(r)$ is the rotation velocity at the radius of r after correcting the inclination as $1/\sin i$. If the gas surface density, Σ_{gas} , exceeds the threshold, Σ_{crit} , then a uniform gas disk is unstable to form rings or clumps which can ultimately collapse into dense molecular gas fragments and form stars, eventually. This criterion, for local gravitational stability in thin isothermal disks, is often expressed as $Q = \Sigma_{\text{crit}}/\Sigma_{\text{gas}}$ (Toomre's Q parameter; Toomre 1964); $Q > 1$ ($Q < 1$) means the gas disk is stable (unstable).

Surprisingly, this criterion has been successfully applied to much smaller scale disks, i.e., inner a few $\times 100$ pc regions of galaxies, to explain the star-formation properties of starbursts (e.g., NGC 3504, Kenney et al. 1993) and rather normal (e.g., NGC 4414, Sakamoto 1996) galaxies. It is therefore natural to expect that the gravitational instabilities of molecular gas would be related to dense molecular gas formation. In fact, Kohno et al. (1999) reported that $R_{\text{HCN/CO}}$ is enhanced in regions where the Q parameter is almost equal to or smaller than unity, suggesting a connection between dense gas formation and gravitational instabilities of molecular gas.

In order to assess the stability of a molecular gas disk in the center of NGC 5195, we calculated Σ_{crit} in NGC 5195 using the above equations. The circular rotation velocities, obtained from the pv map in figure 6, were employed to compute the epicyclic frequency, κ .

¹ In the case of a purely gaseous disk, α is unity. Yet α could be less than unity for a realistic two-fluid stability condition because the interaction between the stellar and gaseous disks could act to destabilize the gas disk (Jog, Solomon 1984). Martin and Kennicutt (2001) has shown that the best-fit value of α is 0.69 ± 0.2 ; we use this in the following calculation.

Note that our interest is just at the center of the gas disk, and that the gas motion can be treated as a rigid rotation in this region. In this case, the epicyclic frequency can be written just as

$$\kappa = \sqrt{2} \left[\frac{v(r)}{r} \right]. \quad (8)$$

From the pv map in figure 6, we suppose that the largest circular rotation velocity occurs at about $r \sim 1''$ or 50 pc and the $v(r)_{\max}$ is about $100 \text{ km s}^{-1}/\sin i = 160 \text{ km s}^{-1}$, yielding a κ of 4.5 within $r < 50$ pc. Note that κ must be a lower limit because the radius of $1''$ where the rotation rises to its peak could be an upper limit, given our limited angular resolution ($\sim 2''$). Concerning the velocity dispersion of molecular gas, we here assumed an intrinsic gas velocity dispersion, σ_v , of 30 km s^{-1} , which is similar to those in NGC 3504 (Kenney et al. 1993). This is because a precise extraction of intrinsic gas velocity dispersion from the observed CO line width (figure 9) is not easy near the center of galaxies due to contamination of the steep velocity gradient within the observing beam. Consequently, we find a critical density, Σ_{crit} , of $6.9 \times 10^3 M_{\odot} \text{ pc}^{-2}$, and that the $Q = \Sigma_{\text{crit}}/\Sigma_{\text{gas}}$ is larger than unity (1.9) in the center of NGC 5195. Hence, the molecular gas disk in the center of NGC 5195 would be gravitationally *stable*; we suggest that this may be the reason why dense molecular gas is not formed from the large amount of diffuse molecular gas in NGC 5195, since they are *too stable to form dense molecular clouds via gravitational instabilities of a diffuse molecular medium*.

Although there are some sources of error, we regard this conclusion as begin rather robust. Though one of the major uncertainties of the Q parameter comes from X_{CO} , recent studies tend to show *smaller* values than the X_{CO} we adopted here by a factor of 2 – 3 or more in the central regions of various galaxies (e.g., Nakai, Kuno 1995; Regan 2000), including the Galactic Center (e.g., Oka et al. 1998; Dahmen et al. 1998). Even in the solar neighborhood, the latest extensive CO survey data of the Milky Way suggest a X_{CO} of $1.8 \times 10^{20} \text{ cm}^{-2} (\text{K km s}^{-1})^{-1}$ (Dame et al. 2001), which is indeed smaller than the X_{CO} adopted in our calculation. Thus the uncertainty of X_{CO} does not weaken our conclusion. Although another source of error is the velocity dispersion, a large velocity dispersion of up to a few $\times 10 \text{ km s}^{-1}$ can be observed even in rather quiescent galaxies; the Galactic Center is the case (e.g., Spergel, Blitz 1992). Given the finite spatial resolution, the epicycle frequency, κ , could be a lower limit, indicating that the critical density can be even larger. It increases the Q value then. All of these error sources thus indicate that the molecular gas in the center of NGC 5195 is indeed supercritical ($Q > 1$) despite the large molecular gas mass there.

Supercritical ($Q > 1$) molecular gas in post-starburst galaxies has also been reported at the centers of NGC 4736 (Shioya et al. 1996) and NGC 7331 (Tosaki, Shioya 1997); both of them are prototypical post-starbursts (see Taniguchi et al. 1996 and reference therein for NGC 4736, and see Ohya, Taniguchi 1996 for NGC 7331). Gravitational instabilities of molecular gas may, therefore, be closely related to dense molecular gas formation and, in turn, massive

star-formation in galaxies.

4.3. *Star-Formation Properties in Early-Type Galaxies*

It should also be addressed why the molecular gas disk in NGC 5195 is supercritical. As mentioned above, the gas surface density, Σ_{gas} , is rather comparable to those in nuclear starburst regions of galaxies. The major difference between starbursts and the post-starburst galaxy NGC 5195 may be the very high critical density for the gravitational instability; the deduced Σ_{crit} of $6.9 \times 10^3 M_{\odot} \text{pc}^{-2}$ is significantly high compared with the central gas surface density in disk galaxies (e.g., Sakamoto et al. 1999b).

This very high threshold may be caused by the large mass concentration in early-type galaxies (Kennicutt 1989). The large concentration of matter results in a steep rise of the rotation velocity, as observed in NGC 5195. This increases the threshold density, because κ becomes very high in this case. In other words, molecular gas at the centers of early-type galaxies tends to be stabilized due to a small gas mass-to-dynamical mass ratio, $M_{\text{gas}}/M_{\text{dyn}}$, even if a significant molecular gas mass concentration, comparable to late-type disk galaxies, occurs (e.g., Young, Scoville 1991).

These properties observed in the S0 galaxy NGC 5195 may explain the difference in the star-formation properties along the Hubble sequence. As reviewed by Kennicutt (1998b), it is now established that the detection frequency of nuclear star formation is lower in early-type galaxies than in late-type ones (e.g., the detection rate is about 8% in S0, whereas it increases about 50% in Sb and reaches 80% in Sc-Im; Ho et al. 1997b), whereas the strength of nuclear star formation shows the opposite trend (i.e., the average extinction-corrected H α luminosities in S0-Sbc galaxies is nine-times higher than in Sc galaxies; Ho et al. 1997b). The high critical density due to the high mass concentration in early-type galaxies may explain these apparently incoherent trends; in early-type galaxies, the occurrence of nuclear star formation is low because nuclear star formation cannot occur until the gas surface density exceeds the higher threshold density compared with late-type galaxies. In order to exceed the threshold, it may take a longer time or many triggers to transport the larger amount of molecular gas into the centers of early-type galaxies. Once the gas surface density exceeds the threshold, however, the star-formation rate must be very high, because the gas surface density already reaches a very high value compared with late-type galaxies (Kennicutt 1989). Our high-resolution CO observations of the early type galaxy NGC 5195 do support this scenario. A CO survey of early-type galaxies using millimeter-wave interferometers and a comparison of the gas surface and the threshold densities with those in late-type spirals must be valuable to statistically test the picture described above regarding the difference in star formation along the Hubble sequence.

5. Summary

We present high-resolution CO(1–0) and HCN(1–0) observations of the Post-Starburst galaxy NGC 5195 made with the Nobeyama Millimeter Array and the NRO 45 m telescope. Our results and conclusions are summarized as follows:

1. We detected strong CO emission in the center of NGC 5195, whereas HCN emission was found to be very weak. The HCN-to-CO integrated intensity ratio in brightness temperature scale, $R_{\text{HCN/CO}}$, is about 0.02. This $R_{\text{HCN/CO}}$ is very small compared with starburst galaxies by a factor of about 5 – 15.
2. Our NMA map of CO emission reveals a concentrated CO distribution toward the nucleus, where little massive star formation is observed; The molecular gas mass per unit area reaches about $\Sigma_{\text{gas}} \sim 3.7 \times 10^3 M_{\odot} \text{ pc}^{-2}$, which is comparable to those in nearby starburst galaxies, whereas the massive star formation rate in the center is smaller than those in typical starburst galaxies by orders of magnitude. The resultant gas consumption time scale, τ_{gas} , is about $\sim 9 \times 10^{10}$ yr, showing very small star-formation efficiency in the center of NGC 5195 compared with that of starburst galaxies.
3. We suggest that the very small $R_{\text{HCN/CO}}$ value could explain the reason why the starburst in NGC 5195 has ceased; most of the dense molecular cores, which are the very sites of massive star-formation, have been consumed away by starburst events which began about 1 Gyr before. A burst of massive star formation can no longer last, although a large amount of *diffuse* molecular gas remains there.
4. We have found a steep rise of rotation velocity toward the center of NGC 5195. It reaches about 160 km s^{-1} at $r \sim 50 \text{ pc}$ on the plane of the galaxy. As a consequence, the critical gas surface density for gravitational instability of the gas disk is very high ($\Sigma_{\text{crit}} \sim 6.9 \times 10^3 M_{\odot} \text{ pc}^{-2}$), and we suggest that the gas disk in the center of NGC 5195 is gravitationally stable. Although NGC 5195 contains large quantities of *low density* molecular gas in the center, they must be too stable to form dense molecular clouds via gravitational instabilities of molecular gas.
5. The deduced very high threshold density seems to be due to a high mass concentration in the center of NGC 5195, and may be characteristic of early-type galaxies. If this is the case, the known trends on the occurrence and luminosity of nuclear star formation along the Hubble sequence can be explained naturally.

We would like to thank the referee for the helpful comments that have improved this paper. We acknowledge the NRO staff for operating the telescopes and continuous efforts to improve the performance of the instruments.

References

- Aalto, S., Booth, R. S., Black, J. H., & Johansson, L. E. B. 1995, *A&A*, 300, 369
- Aalto, S., Hüttemeister, S., & Walter, F. 2001, in *ASP Conf. Ser. 249, The Central Kiloparsec of Starbursts and AGN: The La Palma Connection*, ed. J. H. Knapen, J. E. Beckman, I. Shlosman, and T. J. Mahoney (San Francisco: ASP), 626
- Aalto, S., & Rydbeck, G. 2001, in *ASP Conf. Ser. 249, The Central Kiloparsec of Starbursts and AGN: The La Palma Connection*, ed. J. H. Knapen, J. E. Beckman, I. Shlosman, and T. J. Mahoney (San Francisco: ASP), 719
- Barth, A. J., Ho, L. C., Filippenko, A. V., & Sargent, W. L. W. 1998, *ApJ*, 496, 133
- Block, D. L., Bertin, G., Stockton, A., Grosböl, P., Moorwood, A. F. M., & Peletier, R. F. 1994, *A&A*, 288, 365
- Block, D. L., Elmegreen, B. G., Stockton, A., & Sauvage, M. 1997, *ApJ*, 486, L95
- Boulade, O., Sauvage, M., Altieri, B., Blommaert, J., Gallais, P., Guest, S., Metcalfe, L., Okumura, K., et al. 1996, *A&A*, 315, L85
- Cepa, J., Vila-Vilaró, B., Nakai, N., Kohno, K., Kawabe, R. 1998, in *IAU Symp. 184, The Central Regions of the Galaxy and Galaxies*, ed. Y. Sofue (Dordrecht: Kluwer), 241
- Dahmen, G., Hüttemeister, S., Wilson, T. L., & Mauersberger, R. 1998, *A&A*, 331, 959
- Dame, T. M., Hartmann, D., & Thaddeus, P. 2001, *ApJ*, 547, 792
- de Vaucouleurs, G., de Vaucouleurs, A., Corwin, H. G., Jr., Buta, R. J., Paturel, G., & Fouque, P. 1991, *Third Reference Catalogue of Bright Galaxies* (New York: Springer-Verlag)
- Downes, D., Radford, S. J. E., Guilloteau, S., Guélin, M., Greve, A., & Morris, D. 1992, *A&A*, 262, 424
- Ehle, M., Pietsch, W., & Beck, R. 1995, *A&A*, 295, 289
- Filippenko, A. V., & Sargent, W. L. W. 1985, *ApJS*, 57, 503
- Georgantopoulos, I., Panessa, F., Akylas, A., Zezas, A., Cappi, M., & Comastri, A. 2002, *A&A*, 386, 60
- Greenawalt, B., Walterbos, R. A. M., Thilker, D., & Hoopes, C. G. 1998, *ApJ*, 506, 135
- Ho, L. C., Filippenko, A. V., & Sargent, W. L. W. 1997a, *ApJS*, 112, 315
- Ho, L. C., Filippenko, A. V., & Sargent, W. L. W. 1997b, *ApJ*, 487, 579
- Helfer, T., & Blitz, L. 1993, *ApJ*, 419, 86
- Helfer, T. T., & Blitz, L. 1995, *ApJ*, 450, 90
- Helfer, T. T., & Blitz, L. 1997, *ApJ*, 478, 162
- Hummel, E., van der Hulst, J. M., Keel, W. C., & Kennicutt, R. C., Jr. 1987, *A&AS*, 70, 517
- Jackson, J. M., Heyer, M. H., Paglione, T. A. D., & Bolatto, A. D. 1996, *ApJ*, 456, L91
- Jog, C. J., & Solomon, P. M. 1984, *ApJ*, 276, 114
- Kenney, J. D. P., Wilson, C. D., Scoville, N. Z., Devereux, N. A., & Young, J. S. 1992, *ApJ*, 395, L79
- Kenney, J. D. P., Carlstrom, J. E., & Young, J. S. 1993, *ApJ*, 418, 687
- Kennicutt, R. C., Jr. 1983, *ApJ*, 272, 54
- Kennicutt, R. C., Jr. 1989, *ApJ*, 344, 685
- Kennicutt, R. C., Jr. 1998a, *ApJ*, 498, 541
- Kennicutt, R. C., Jr. 1998b, *ARA&A*, 36, 189

- Kohno, K., Kawabe, R., Tosaki, T., & Okumura, S. K. 1996, *ApJ*, 461, L29
- Kohno, K., Kawabe, R., & Vila-Vilaró, B. 1999, *ApJ*, 511, 157
- Kohno, K., Matsushita, S., Vila-Vilaró, B., Okumura, S. K., Shibatsuka, T., Okiura, M., Ishizuki, S., & Kawabe, R. 2001, in *ASP Conf. Ser. 249, The Central Kiloparsec of Starbursts and AGN: The La Palma Connection*, ed. J. H. Knapen, J. E. Beckman, I. Shlosman, and T. J. Mahoney (San Francisco: ASP), 672 (astro-ph/0206398)
- Martin, C. L., & Kennicutt, R. C., Jr. 2001, *ApJ*, 555, 301
- Nakai, N., & Kuno, N. 1995, *PASJ*, 47, 761
- Noguchi, M. 1996, *ApJ*, 469, 605
- Ohyama, Y., & Taniguchi, Y. 1996, in *ASP Conf. Ser. 103, The Physics of LINERs in view of recent observations*, ed. M. Eracleous, A. Koratkar, C. Leitherer, L. Ho (San Francisco: ASP), 205
- Oka, T., Hasegawa, T., Hayashi, M., Handa, T., & Sakamoto, S. 1998, *ApJ*, 493, 730
- Okumura, S. K., Momose, M., Kawaguchi, N., Kanzawa, T., Tsutsumi, T., Tanaka, A., Ichikawa, T., Suzuki, T., et al. 2000, *PASJ*, 52, 393
- Paglione, T. A. D., Jackson, J. M., & Ishizuki, S. 1997, *ApJ*, 484, 656
- Paglione, T. A. D., Tosaki, T., & Jackson, J.M. 1995, *ApJ*, 454 L117
- Pritchett, C. 1977, *ApJS*, 35, 397
- Regan, M. W. 2000, *ApJ*, 541, 142
- Regan, M. W., Sheth, K., & Vogel, S. N. 1999, *ApJ*, 526, 97
- Reynaud, D., & Downes, D. 1997, *A&A*, 319, 737
- Rieke, G. H. 1988, in *Galactic and Extragalactic Star Formation*, ed. R.E. Pudritz, M. Fich (Dordrecht: Kluwer), 561
- Rieke, G. H., Lebofsky, M. J., & Walker, C. E. 1988, *ApJ*, 325, 679
- Rots, A. H., Bosma, A., van der Hulst, J. M., Athanassoula, E., & Crane, P. C. 1990, *AJ*, 100, 387
- Sage, L. J. 1989, *ApJ*, 344, 200
- Sage, L.J. 1990, *A&A*, 239, 125
- Sage, L. J., & Wrobel, J. M. 1989, *ApJ*, 344, 204
- Sakamoto, K. 1996, *ApJ*, 471, 173
- Sakamoto, K., Okumura, S. K., Ishizuki, S., Scoville, N. Z. 1999a, *ApJS*, 124, 403
- Sakamoto, K., Okumura, S. K., Ishizuki, S., Scoville, N. Z. 1999b, *ApJ*, 525, 691
- Sakamoto, K., Okumura, S. K., Minezaki, T., Kobayashi, Y., & Wada, K. 1995, *AJ*, 110, 2075
- Sandage, A., & Tammann, G. A. 1981, *A Revised Sharpley–Ames Catalog of Bright Galaxies* (Washington: Carnegie Institution of Washington)
- Sauvage, M., Blommaert, J., Boulanger, F., Cesarsky, C. J., Cesarsky, D. A., Désert, F. X., Elbaz, D., Gallais, G., et al. 1996, *A&A*, 315, L89
- Scoville, N. Z., Yun, M. S., Clemens, D. P., Sanders, D. B., Waller, W. H. 1987, *ApJS*, 63, 821
- Shioya, Y., Tosaki, T., Ohyama, Y., Murayama, T., Yamada, T., Ishizuki, S., & Taniguchi, Y. 1998, *PASJ*, 50, 317
- Shlosman, I., Frank, J., & Begelman, M. C. 1989, *Nature*, 338, 45
- Smith, J., Gehrz, R. D., Grasdalen, G. L., Hackwell, J. A., Dietz, R. D., & Friedman, S. D. 1990, *ApJ*, 362, 455

- Solomon, P. M., Downes, D., & Radford, S. J. E. 1992, *ApJ*, 387, L55
- Solomon, P. M., Rivolo, A. R., Barrett, J., & Yahil, A. 1987, *ApJ*, 319, 730
- Sorai, K., Nakai, N., Kuno, N., & Nishiyama, K. 2002, *PASJ*, 54, 179
- Sorai, K., Nakai, N., Kuno, N., Nishiyama, K., & Hasegawa, T. 2000, *PASJ*, 52, 785
- Spergel, D. N., & Blitz, L. 1992, *Nature*, 357, 665
- Spillar, E. J., Oh, S. P., Johnson, P. E., & Wenz, M. 1992, *AJ*, 103, 793
- Tacconi, L. J., Tacconi-Garman, L. E., Thornley, M., & van Woerden, H. 1991, *A&A*, 252, 541
- Taniguchi, Y., Murayama, T., Nakai, N., Suzuki, M., & Kameya, O. 1994, *AJ*, 108, 468
- Taniguchi, Y., Ohyama, Y., Yamada, T., Mouri, H., & Yoshida, M. 1996, *ApJ*, 467, 215
- Thornley, M. D., Schreiber, N. M. F., Lutz, D., Genzel, R., Spoon, H. W. W., Kunze, D., & Sternberg, A. 2000, *ApJ*, 539, 641
- Thronson, H. A., Jr., Rubin, H., & Ksir, A. 1991, *MNRAS*, 252, 550
- Thronson, H. A., Jr., Tacconi, L., Kenney, J., Greenhouse, M. A., Margulis, M., Tacconi-Garman, L., & Young, J. S. 1989, *ApJ*, 344, 747
- Toomre, A. 1964, *ApJ*, 139, 1217
- Tosaki, T., & Shioya, Y. 1997, *ApJ*, 484, 664
- Tsutsumi, T., Morita, K. -I., & Umeyama, S. 1997, in *ASP Conf. Ser. 125, Astronomical Data Analysis Software and Systems VI*, ed. G. Hunt, H.E. Payne (San Francisco: ASP), 50
- Tully, R. B. 1988, *Nearby Galaxies Catalog* (Cambridge: Cambridge University Press)
- van der Hulst, J. M., Kennicutt, R. C., Crane, P. C., & Rots, A. H. 1988, *A&A*, 195, 38
- Walker, C. E., Lebofsky, M. J., & Rieke, G. H. 1988, *ApJ*, 325, 687
- Wrobel, J. M., & Kenney, J. D. P. 1992, *ApJ*, 399, 94
- Yamada, T., & Tomita, A. 1996, in *Ground-Based Astronomy in Asia*, ed. N. Kaifu (Tokyo: University Academy Press), 268
- Young, J. S., & Scoville, N. Z. 1991, *ARA&A*, 29, 581
- Zhao, J. -H., Anantharamaiah, K. R., Goss, W. M., & Viallefond, F. 1996, *ApJ*, 472, 54

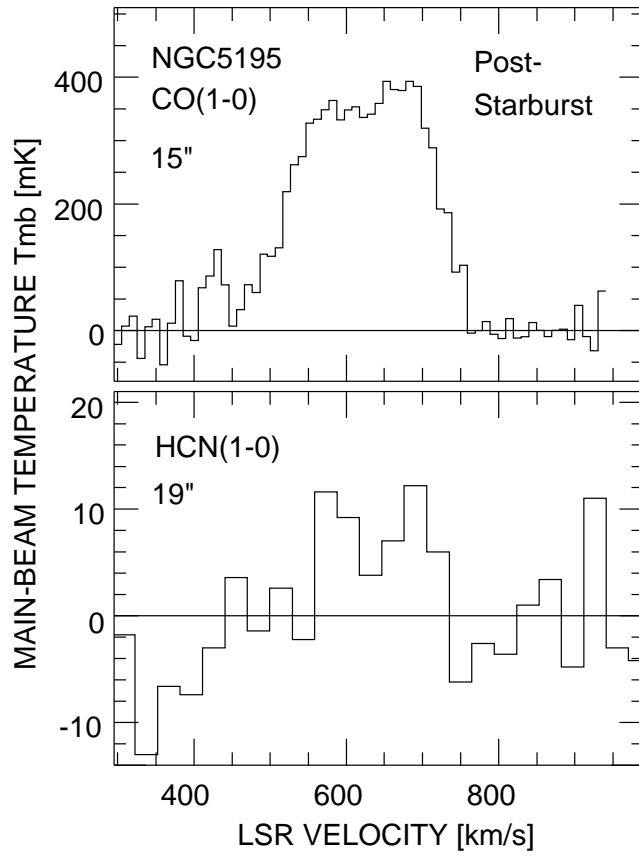


Fig. 1. CO(1–0) and HCN(1–0) spectra in the center of NGC 5195 obtained with the NRO 45 m telescope. The beam sizes (HPBW) of the CO and HCN data are 15'' and 19'', respectively.

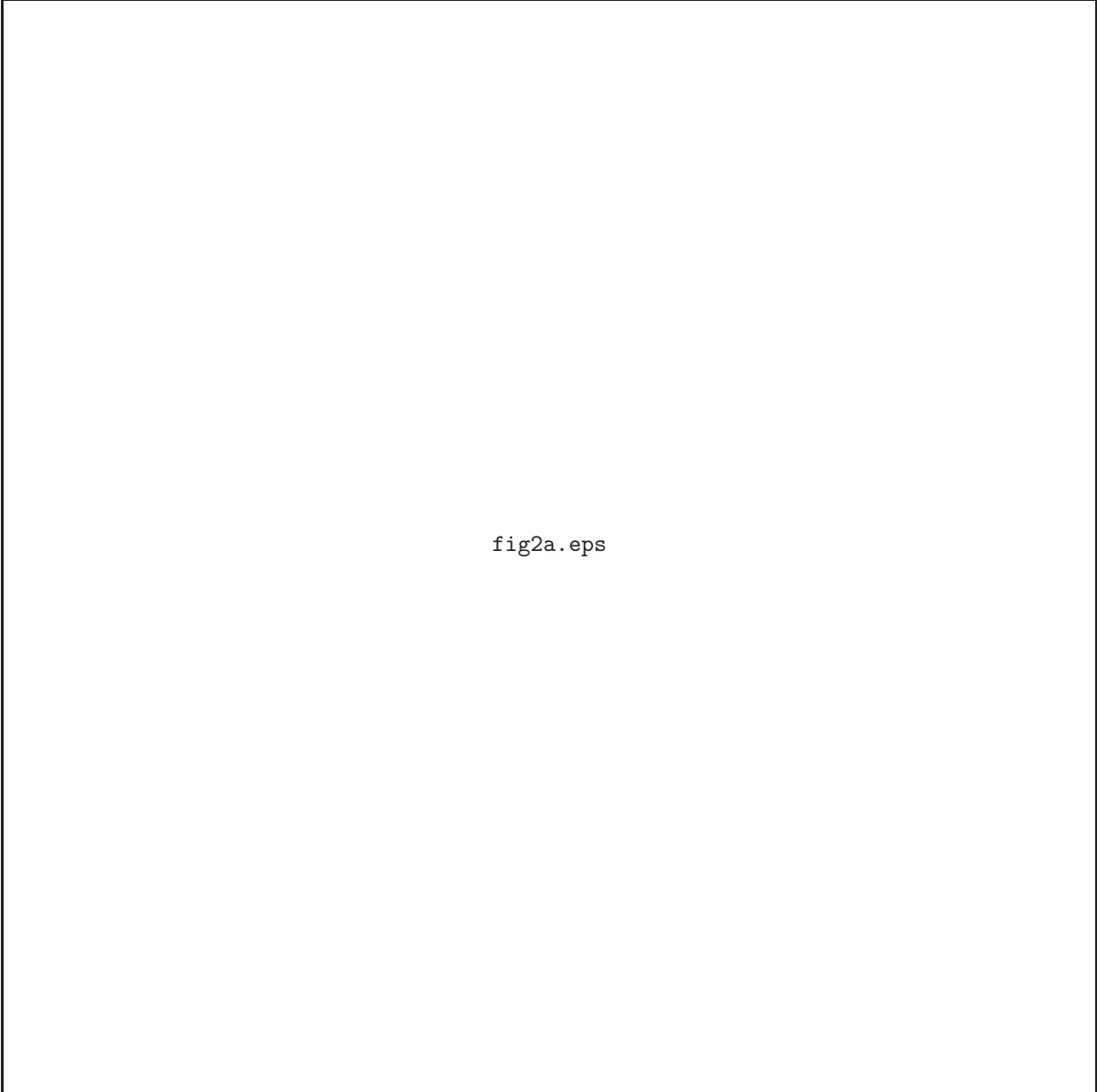


fig2a.eps

Fig. 2. CO(1–0) emission in 15.6 km s^{-1} wide channels from the central $50'' \times 50''$ region (2.25 kpc at $D = 9.3 \text{ Mpc}$) of NGC 5195 observed with the NMA. The synthesized beam is $4.''7 \times 3.''2$ ($210 \times 140 \text{ pc}$) with a P.A. of -54° (the low resolution map). The contour levels are $-4, -2, 2, 4, 6, \dots, 16$, and 18σ , where $1 \sigma = 23 \text{ mJy beam}^{-1}$ or 140 mK in T_b . Negatives are dashed, and zero contour is omitted. The cross indicates the position of the phase center, which corresponds to the peak position of 6 cm radio continuum. NMA field of view ($60''$) is also indicated. The attenuation of the 10 m dish is not corrected in these maps.

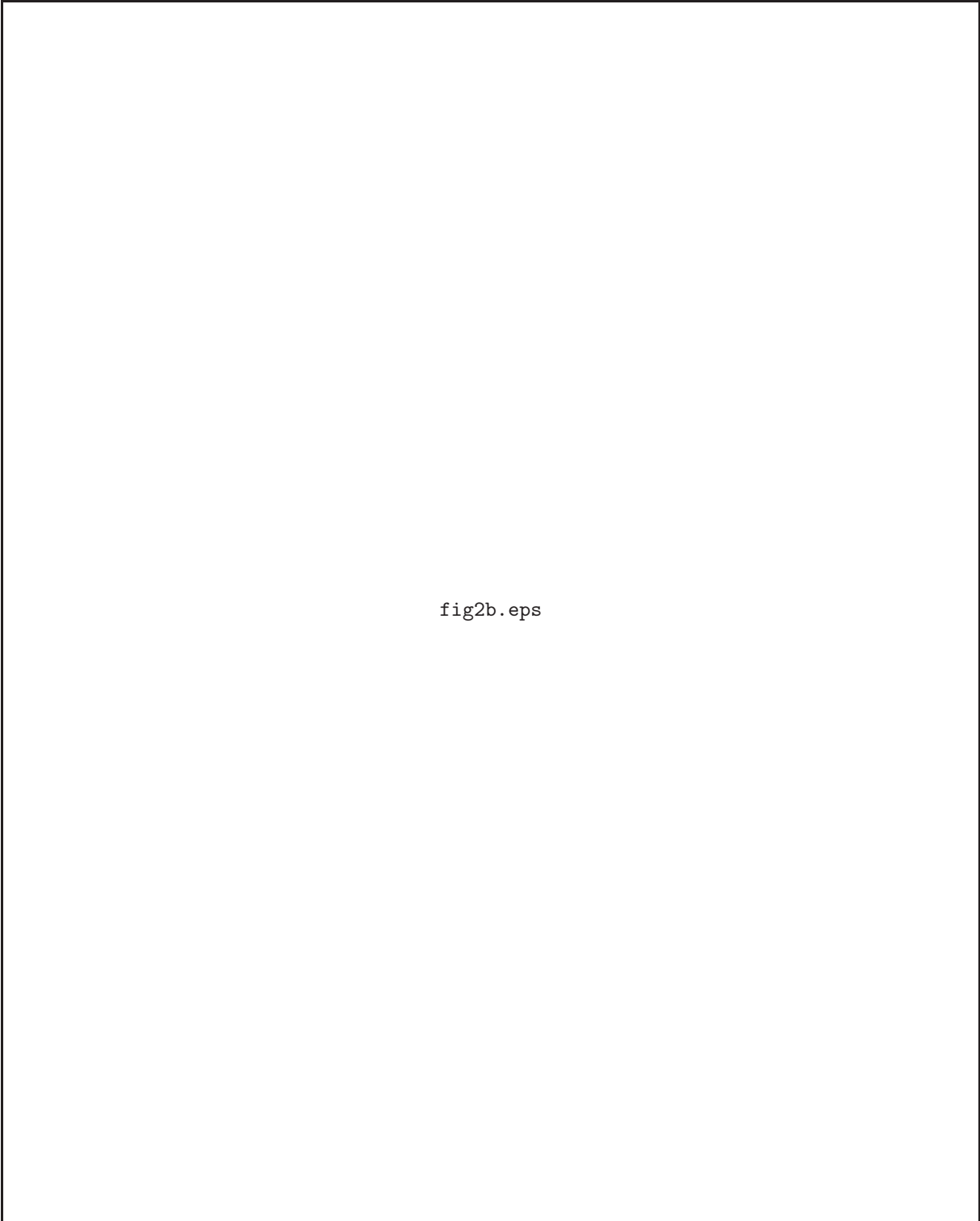


fig2b.eps

Fig. 2. (Continued)

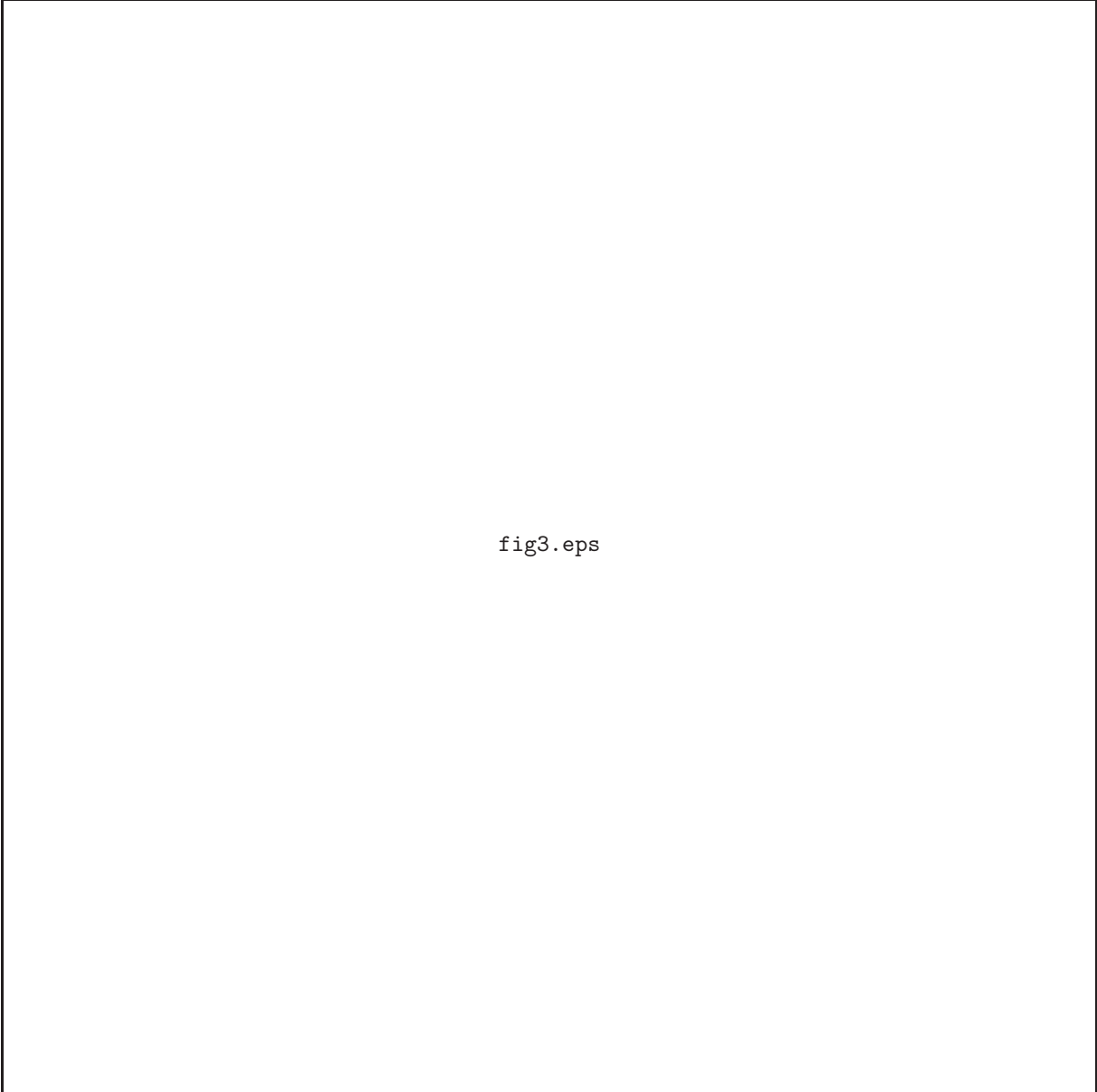


fig3.eps

Fig. 3. High-resolution CO(1–0) integrated intensity and mean-velocity maps along with optical (broad band and narrow band) images of NGC 5195; (a) DSS *B*-band image of NGC 5195. The central $3' \times 2.5'$ is shown, and the NMA field of view ($60''$) is superposed on the picture as a dashed circle. The solid box corresponds to the CO map region below. (b) Pseudo-color H α + [N II] image of NGC 5195 (Greenawalt et al. 1998). The contour levels are $-300, -100, -30, -10, 10, 30, 100,$ and 300σ , where $1 \sigma = 2.4 \times 10^{17}$ erg s $^{-1}$ cm $^{-2}$ arcsec $^{-2}$. Negatives are dashed. NMA field of view is indicated (dashed circle). Note the strong absorption toward the center of NGC 5195 (the central cross) with a diameter of about $10''$ or 450 pc. (c) High-resolution integrated intensity map of CO(1–0) emission from the central $30'' \times 25''$ region (1.35 kpc \times 1.13 kpc) of NGC 5195. The synthesized beam is $1''.9 \times 1''.8$ (86 pc \times 81 pc) with a P.A. of -48° . The contour levels are $2, 4, 6, 8, 10, 15,$ and 20σ , where $1 \sigma = 1.5$ Jy beam $^{-1}$ km s $^{-1}$ or 39.4 K km s $^{-1}$ in T_b . The 1σ corresponds to the face-on gas surface density, Σ_{gas} , of $190 M_\odot$ pc $^{-2}$. (d) Intensity-weighted mean velocity map of CO(1–0) emission. The contour interval is 20 km s $^{-1}$.

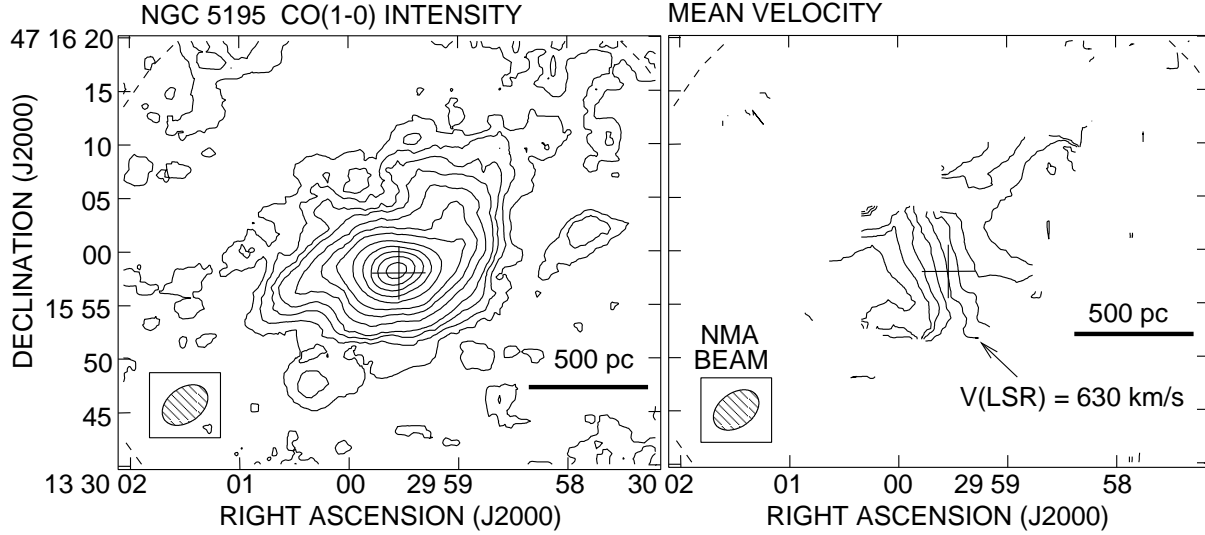


Fig. 4. Low resolution CO data of NGC 5195. (left) Integrated intensity map of CO. The synthesized beam is $4''.7 \times 3''.2$ ($210 \text{ pc} \times 140 \text{ pc}$) with a P.A. of -54° . The contour levels are 1.5, 3, 4.5, 6, 9, 12, 15, 20, 25, 30, 35, 40, and 45σ , where $1 \sigma = 1.5 \text{ Jy beam}^{-1} \text{ km s}^{-1}$ or 9.3 K km s^{-1} in T_b . This corresponds to a face-on gas surface density, Σ_{gas} , of $48.8 M_\odot \text{ pc}^{-2}$. (right) Intensity weighted mean velocity map of CO. The contour interval is 20 km s^{-1} .

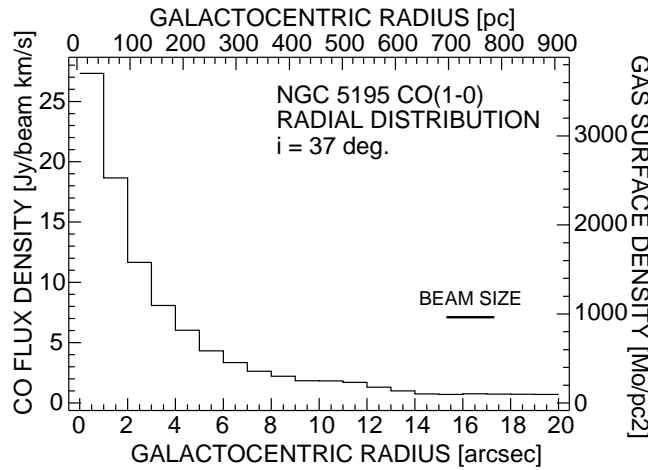


Fig. 5. Radial distribution of CO emission in the central $r < 25''$ (1.1 kpc) region of NGC 5195. The high-resolution CO integrated intensity map (figure 4) is azimuthally averaged over the successive annuli with a $1'' = 45 \text{ pc}$ width. Corrections for the inclination and primary beam attenuation are applied. The face-on gas surface density was calculated by adopting a conversion factor of $X_{\text{CO}} = 3.0 \times 10^{20} \text{ cm}^{-2} (\text{K km s}^{-1})^{-1}$, including heavier elements. A strong gas concentration toward the nucleus is evident.

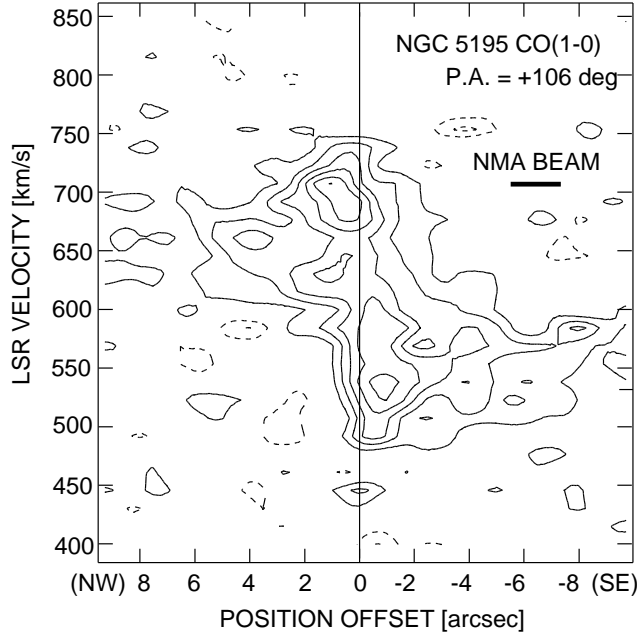


Fig. 6. Position-to-Velocity (pv) map of CO emission along the P.A. of $+106^\circ$ (measured counterclockwise from N), i.e., the kinematical major axis determined from the CO velocity field. This pv map is derived from the high-resolution CO data cube. A correction of inclination was not applied, whereas a primary beam correction was applied. The origin of position offset corresponds to $\alpha(\text{J2000}) = 13^{\text{h}}29^{\text{m}}59^{\text{s}}54$ and $\delta(\text{J2000}) = +47^\circ15'58''.0$. The contour levels are $-3, -1.5, 1.5, 3, \dots, 9 \sigma$, where $1 \sigma = 22 \text{ mJy beam}^{-1}$.

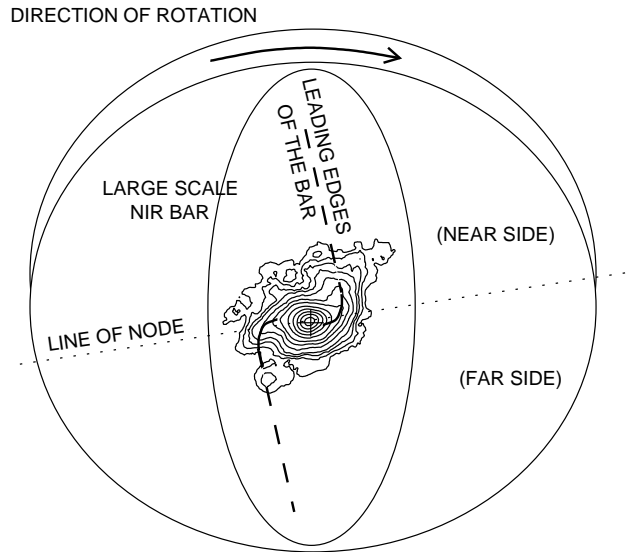


Fig. 7. Schematic view of NGC 5195. This is based on the assumption that the observed CO structures, such as two offset ridges emanating from the nuclear peak and curved/spiral-like structures, are driven by a large-scale stellar bar, which is clearly identified in the NIR bands.

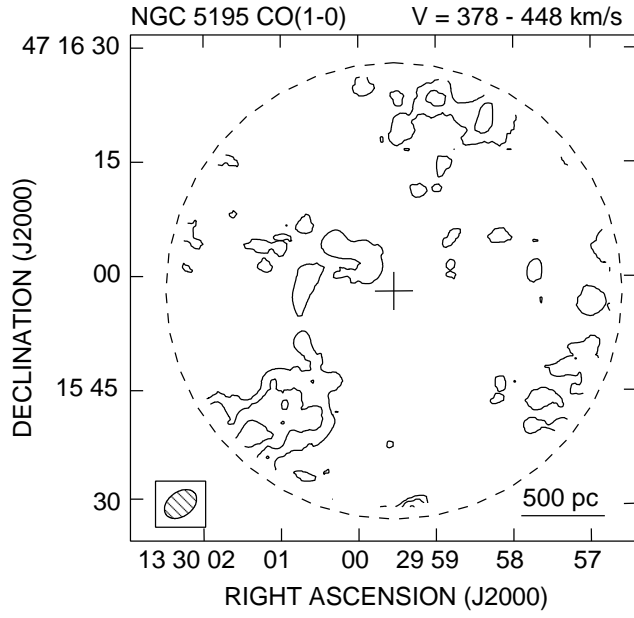


Fig. 8. Integrated intensity map of CO emission over the velocity range $V_{\text{LSR}} = 378 - 448 \text{ km s}^{-1}$, showing CO emission possibly from a spiral arm of M 51. This map was produced from the low-resolution CO cube. The contour levels are 2, 4, and 6 σ , where 1 $\sigma = 0.80 \text{ Jy beam}^{-1} \text{ km s}^{-1}$ or 4.9 K km s^{-1} in T_{b} , corresponding to a face-on gas surface density of $\Sigma_{\text{gas}} = 26 M_{\odot} \text{ pc}^{-2}$, including heavier elements as $\Sigma_{\text{gas}} = 1.36 \times \Sigma_{\text{H}_2}$. The primary beam attenuation was corrected.

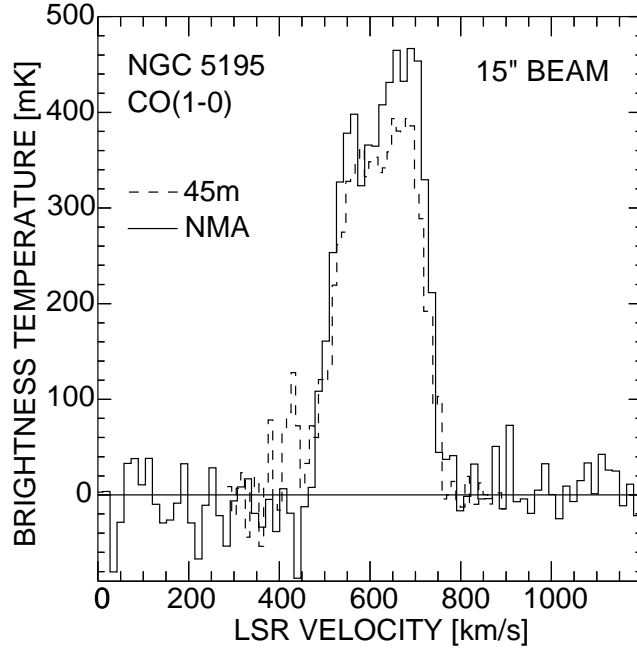


Fig. 9. Comparison of the CO spectra taken with the NMA and 45 m. The NMA spectrum was made after convolving the low-resolution CO data cube to the same beam size as the 45 m beam (15"). Note that low-velocity component (near 400 km s⁻¹) seen in the 45 m spectrum is not evident in the NMA cube, suggesting that this velocity component distributes widely beyond the NMA F.O.V. and would be mostly resolved out in the NMA data.

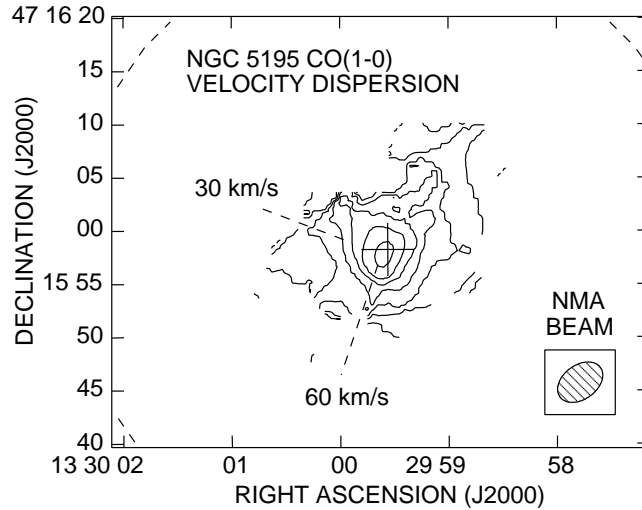


Fig. 10. Intensity-weighted velocity dispersion map of the CO emission in NGC 5195, which was computed by calculating the second-order moment of intensity from the low-resolution CO cube. The contour interval is 10 km s⁻¹. Note that this map contains both the intrinsic gas velocity dispersion and the gradient of rotation velocity across the observing beam.

Table 1. Parameters of NGC 5195.

Parameter	Value	Reference
Morphology	IA0 pec	(a)
	SB0 pec	(b)
Size ($D_{25} \times d_{25}$)	$5'8 \times 4'6$	(a)
Nuclear activity	L2:	(c)
	post-starburst	(d), (e)
Position of nucleus		(f)
α (J2000)	$13^{\text{h}}29^{\text{m}}59^{\text{s}}54$	
α (J2000)	$+47^{\circ}15'58''0$	
Position angle	$+101^{\circ}$ (counterclockwise from N)	(a)
Inclination angle	37° (face-on = 0°)	(a)
Distance	9.3 Mpc	(g)
Liner scale	$45.1 \text{ pc arcsec}^{-1}$	
H α luminosity ($2'' \times 4''$ area) ...	$8.7 \times 10^{37} \text{ erg s}^{-1}$	(c)
SFR per unit area [†] Σ_{SFR}	$3.7 \times 10^{-8} M_{\odot} \text{ pc}^{-2} \text{ yr}^{-1}$	

References: (a) de Vaucouleurs et al. 1991, RC3; (b) Sandage, Tammann 1981, RSA; (c) Ho et al. 1997a; (d) Rieke 1988; (e) Boulade et al. 1996; (f) Hummel et al. 1987; (g) Tully 1988.

[†] Star formation rate (SFR) was derived as $L_{\text{H}\alpha}/(1.12 \times 10^{41} \text{ erg s}^{-1})$ in $M_{\odot} \text{ yr}^{-1}$ (Kennicutt 1983). No correction for extinction was made.

Table 2. NRO 45 m observations.

Parameter	CO(1–0)	HCN(1–0)
Beamsize (FWHP)	$15''$	$19''$
Main beam efficiency η_{MB}	0.5	0.5
Velocity resolution Δv [km s^{-1}]	10	30
Peak temperature in T_{MB} [mK]	$4.0 \times 10^2 \pm 24$	12 ± 5.2
Integrated intensity [†] $\int T_{\text{MB}}(v)dv$ [K km s^{-1}]	83 ± 1.4	1.5 ± 0.60
Luminosity L' [$\text{K km s}^{-1} \text{ pc}^2$]	3.8×10^7	1.3×10^6

[†] Integrated over the velocity range of $V_{\text{LSR}} = 450 - 750 \text{ km s}^{-1}$.

Table 3. NMA observations.

Parameter	Value
Field of view (FWHP)	60''
	2.7 kpc at $D = 9.3$ Mpc
Bandwidth	512 MHz
Visibility calibrator	1418+546
Flux density of calibrator	0.5 – 0.7 Jy
Array configuration	AB, C, and D
low resolution CO cube	
Weighting	Natural, 80 k λ taper
Synthesized beam	4''7 \times 3''2, -54°
	210 pc \times 140 pc
Equivalent T_b for 1 Jy beam $^{-1}$	6.1 K (Jy beam $^{-1}$) $^{-1}$
Velocity resolution Δv	15.6 km s $^{-1}$
rms noise level in channel maps	23 mJy beam $^{-1}$
CO flux within the F.O.V.	340 \pm 9.1 Jy km s $^{-1}$
Molecular gas mass within the F.O.V. †	4.8 \times 10 8 M_\odot
Peak face-on gas surface density †	2.0 \times 10 3 M_\odot pc $^{-2}$
CO intensity at 15'' beam ‡	93.2 K km s $^{-1}$
$I(\text{NMA})/I(45\text{m})^\ddagger$	1.1
high resolution CO cube	
Weighting	Robust (robustness 0)
Synthesized beam	1''9 \times 1''8, -48°
	86 pc \times 81 pc
Equivalent T_b for 1 Jy beam $^{-1}$	27 K (Jy beam $^{-1}$) $^{-1}$
Velocity resolution Δv	15.6 km s $^{-1}$
rms noise level in channel maps	22 mJy beam $^{-1}$

† Adopting a conversion factor $X_{\text{CO}} = 3.0 \times 10^{20} \text{ cm}^{-2} (\text{K km s}^{-1})^{-1}$.

‡ The NMA CO cube was convolved with 15'' beam (the same as the 45 m observations) and CO intensity at the center (the observed position with the 45 m), integrated over the velocity range of $V_{\text{LSR}} = 471 - 752 \text{ km s}^{-1}$, was compared with the 45 m data (table 2). Most of the single dish flux seems to be recovered in this velocity range.

This figure "fig2a.gif" is available in "gif" format from:

<http://arxiv.org/ps/astro-ph/0206400v1>

This figure "fig2b.gif" is available in "gif" format from:

<http://arxiv.org/ps/astro-ph/0206400v1>

This figure "fig3.gif" is available in "gif" format from:

<http://arxiv.org/ps/astro-ph/0206400v1>